

Particle Entrapment in the Mushy Region of a Steel Continuous Caster

C. Pfeiler¹, B.G. Thomas², A. Ludwig¹, M. Wu¹

¹ Christian-Doppler Laboratory for Multiphase Modeling of Metallurgical Processes, Department of Metallurgy, University of Leoben, Franz-Josef-Str. 18, A-8700 Leoben, Austria

² Department of Mechanical Science & Engineering, University of Illinois at Urbana-Champaign, 1206 West Green Street, Urbana, IL 61801, USA

ABSTRACT: Avoiding particle entrapment into the solidifying shell of a steel continuous caster is important to improve quality of the continuous cast product. Therefore, the fluid flow dynamics in the steel melt and mushy zone, heat transfer and solidification of the steel shell, as well as the motion and entrapment of inclusion particles during the casting process were investigated using computational models. Solidification of the strand shell is modelled with an enthalpy-formulation by assuming a columnar morphology in the mushy zone. The motion of particles is tracked with a Lagrangian approach. When the particles reach the solidification front they can be entrapped/engulfed into the solid shell or pushed away from the solidification front, depending on the mushy zone morphology and the forces acting on them. The current paper focuses on the mould region at a steel continuous caster, including the submerged entry nozzle (SEN) and 1.2 m length of the strand. The model results demonstrate the potential of the model to predict the positions and the amount of entrapped/engulfed particles in the solidifying strand.

1. INTRODUCTION

Non-metallic particles originate from deoxidation, reoxidation and exogenous reactions during metallurgical processes to refine and transport the molten metal. Continuous casting is a critical step in the production chain of steelmaking and is the last opportunity to remove particles from the steel melt. Therefore, a major concern is to understand the transport and entrapment/engulfment of particles during continuous casting. If the flow in the mould is carefully adjusted, the melt may carry the particles to the liquid slag layer, where they might be removed. Otherwise, they will eventually be trapped by the solidification front and cause undesired defects in the final product. It is pertinent for optimizing process control and product quality to understand the interactions between the solid front and the particles in the melt. Voller [1] derived a solidification model for one phase which includes a special latent heat treatment for columnar solidification. Small-scale studies of solid shell - particle interaction [2, 3] have shown that the particle capture behaviour depends strongly on the shape of the interface and the difference in thermal conductivity of the particle and solidified material. A balance between forces acting between particles, the surrounding fluid, and the solidification front of the continuous caster was derived at the wall by Yuan [4]. The dendritic tip front was defined as the wall boundary. The purpose of the present study is to combine these models into a general model to describe the motion of particles during solidification steel in a continuous caster and to estimate the amount and entrapment positions of those particles in the solidified shell. To validate the present model, comparisons with experimental measurements of the shell thickness are performed.

2. MODEL DESCRIPTION

2.1 Solidification

The energy conservation equation considering solidification is defined as

$$\rho \frac{\partial h}{\partial t} + \rho \nabla(\bar{u}h) = \nabla(k_{eff} \nabla T) + \rho L \frac{\partial f_s}{\partial t} + \rho L \bar{u}_{pull} \nabla f_s. \quad (1)$$

Where, h is the sensitive enthalpy defined as $h_{ref} + \int_{T_{ref}}^T c_p dT$; h_{ref} is the reference enthalpy at the reference temperature T_{ref} and c_p is the specific heat. ρ is the density of the melt, \bar{u} the velocity and k_{eff} is the effective conductivity which is defined as $k_{eff} = k + k_i$.

Here, k defines the thermal conductivity of the material and k_t the turbulent thermal conductivity. The relationship between temperature and solid fraction f_s was calculated with IDS, a commercial solidification analysis package, for the given steel composition of a 434 stainless steel assuming non-equilibrium cooling conditions typical of steel continuous casting.

The mass and momentum conservation equations for the melt are given by

$$\nabla \cdot \vec{u} = 0 \quad (3)$$

$$\frac{\rho \partial \vec{u}}{\partial t} + \rho (\vec{u} \otimes \vec{u}) = -\nabla p + \nabla (\mu_{eff} \nabla \vec{u}) + S \quad (4)$$

where $\mu_{eff} = \mu_l + \mu_t$ is the effective viscosity due to turbulence, for which the standard k - ε model is used. μ_l is the dynamic viscosity and μ_t , the turbulent viscosity, which is defined by $\mu_t = \rho C_\mu k^2 / \varepsilon$ with $C_\mu = 0.09$. p is the static pressure. The pressure drop caused by the presence of solid material is considered as a momentum sink S in the momentum conservation equation. The mushy zone is treated as a porous region with volume fraction of pores equal to the liquid fraction f_l . The momentum sink for steel, applying the Blake-Kozeny law, is taken from [5]:

$$S = \frac{(1 - f_l)^2}{f_l^3} \frac{1660 \mu_l}{\lambda_1^2} (\vec{u} - \vec{u}_{pull}) \quad (5)$$

Here, λ_1 is the primary dendrite arm spacing of the solidified strand. Corresponding sink terms are also added to all of the turbulence equations in the mush and solidified areas.

2.2 Particle tracking

Particles are considered as discrete spheres of a secondary phase dispersed in the melt. The trajectories of these particles are tracked by integrating the equation of motion in a Lagrangian frame of reference considering the drag force, the gravitational force, the lift force F_L , the virtual mass force and the pressure and stress gradient forces, as given in the terms on the right-hand-side (RHS) of the following equation:

$$m_p \frac{d\vec{u}_p}{dt} = \frac{1}{8} \pi d_p^2 \rho_l C_D |\vec{u}_l - \vec{u}_p| (\vec{u}_l + \vec{u}'_l - \vec{u}_p) + \frac{1}{6} \pi d_p^3 \rho_p \vec{g} + F_L + \frac{\rho_l \pi d_p^3}{12} \left(\frac{D\vec{u}_l}{Dt} - \frac{d\vec{u}_p}{dt} \right) + \frac{d_p^3 \pi}{6} \rho_p \frac{D\vec{u}_l}{Dt} \quad (6)$$

The superscripts l and p correspond to the melt and particle respectively. d is the diameter, m the mass, \vec{g} the gravity and \vec{u}'_l is the fluctuating velocity caused by turbulence. The dispersion of particles due to turbulence in the melt is treated using a stochastic tracking model, described in detail elsewhere [6]. The effect of the discrete phase on turbulence is ignored. F_L is described in detail by Yuan [4]. For the drag coefficient, $C_D = (1 + 0.15 \text{Re}_p^{0.687}) / \text{Re}_p$, the approach of Sommerfeld [7] is taken. When the particles approach the solidification front they are entrapped if $d_p < \text{PDAS}$. Otherwise, they are either engulfed or pushed away [4], depending on the dendritic morphology, the flow and the cooling conditions. In the present work this entrapment model is combined with solidification. The area of particle entrapment is, instead of a wall, the liquidus iso-surface, which approximates the dendritic front. These iso-surfaces are defined as planes normal to the temperature gradient. To model particle pushing, the reflection angle of particles equals the incidence angle. The position of each particle that becomes entrapped or engulfed, is recorded before it vanishes from the domain. This has also the advantage of saving CPU time. An example of the force balance normal to the solidification front is shown as

$$\vec{F}_L + \left(\vec{F}_B \cdot \frac{\vec{\nabla} T}{\|\vec{\nabla} T\|} \right) + \left(\vec{F}_D \cdot \frac{\vec{\nabla} T}{\|\vec{\nabla} T\|} \right) > 2(\vec{F}_{Lub} - \vec{F}_{Grad} - \vec{F}_I) \cos(\theta) \quad (7)$$

Here, θ is defined as angle between the normal to the solidification front and the connection line between particle centre and dendrite tip. If the particle is not pushed, that means that the left side of this equation is smaller than the right, so a second force balance is done in the direction normal to the line connecting the particle center and dendrite tip. This decides a second time if pushing or engulfment occurs. Three additional forces act between dendrites and particles: the lubrication force, the interfacial force and the surface energy gradient force. All of these act along the line between the particle centre and the centre of the dendrite tip. To avoid capture, the particle must be pushed by the solid interface at the speed of the continuously growing solidification front, which requires enough melt to flow into the gap between the particle and the dendrites. This creates the lubrication force, which acts on the particle towards the interface, due to this flow around the particle. If the forces due flow into the gap and the solidifying mass are in equilibrium, the particle can be pushed. This flow around the particle causes a low local pressure near the dendrite tips. The lubrication force enhances particle engulfment and is defined near a dendritic front [2] as

$$F_{Lub} = 6\pi\mu_l v_{sol} \frac{R_p^2}{h} \left(\frac{R_d}{R_d + R_p} \right)^2. \quad (8)$$

v_{sol} is the dendrite tip velocity depending on the local cooling conditions, h is the distance between the particle and the dendrite, and is in the order of nanometres. The radius of the particle is R_p and the radius of the dendrite tip is R_d . Due to interfacial energies between the melt (l), the solid (s) and the particle (p), the force pushing the particle into the solid, assuming $R_p \gg h$, is defined as [2]

$$F_I = 2\pi R_p \Delta\sigma_0 \frac{a_0^2}{h^2} \left(\frac{R_d}{R_d + R_p} \right). \quad (9)$$

Here, the resulting interfacial energy between the phases is $\Delta\sigma_0 = \sigma_{sp} - \sigma_{lp} - \sigma_{sl}$. If $\Delta\sigma_0 > 0$ the force is conductive to push the particle. a_0 is the atomic diameter of an iron atom. The surface energy of steel at the dendritic front is mostly affected by sulfur, an interfacial-active element. A steep sulfur concentration gradient ahead of the dendrites, influencing the surface energy of the melt around the particle, tends to encourage particle engulfment. The Surface Energy Gradient Force near a dendritic front derived by Yuan [4] is,

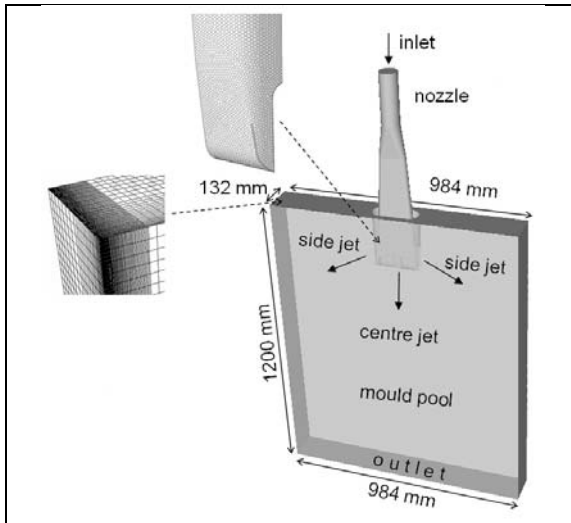
$$F_{Grad} = -\frac{m\beta\pi R_p}{\xi^2} \left\{ \frac{(\xi^2 - R_p^2)}{\beta} \ln \left[\frac{(\xi + R_p)[\alpha(\xi - R_p) + \beta]}{(\xi - R_p)[\alpha(\xi + R_p) + \beta]} \right] + \frac{2R_p}{\alpha} - \frac{\beta}{\alpha^2} \ln \left[\frac{[\alpha(\xi + R_p) + \beta]}{[\alpha(\xi - R_p) + \beta]} \right] \right\} \quad (9)$$

Where $\alpha = 1 + nC_s$, $\beta = nR_d(C^* - C_s)$ and ξ is defined as $\xi = R_p + R_d + h$. C_s is the sulfur concentration in the bulk melt and C^* is the concentration at the solid-liquid interface. n and m are empirical constants with values of 0.17 J/m² and 844 (mass %)⁻¹.

3. SIMULATION DETAILS

Geometry, material properties and some process parameters were adjusted to the measurement conditions shown in Tab. 1. The calculation domain consists of a quarter of the 1.2 m long upper part of the caster including a trifurcated submerged entry nozzle without any geometrical simplifications. The symmetric and stable flow field was demonstrated in former studies [8]. The computation domain is discretized into structured hexahedral and unstructured polyhedral volume elements and consists of 1.2 million cells with a fine graded mesh in the mushy zone. The inlet is positioned at the top surface of the trifurcated nozzle. At the inlet of the calculation domain, a flat velocity profile and at the bottom a constant pressure boundary condition were applied. The top surface of the liquid melt pool being in contact with the casting slag is supposed to be flat. Here, a free-slip condition is used. At the inlet the particles are injected. Particles are modeled as to be caught at the top surface, but in the mushy region of the caster they can be entrapped, engulfed or pushed following the rules of the capture criteria [4]. At the mold walls a heat flux function based on industrial

measurements [8] is used. The solidified shell moves downwards at constant casting speed.

	casting speed [mm/s]	25.4
	pour temperature [K]	1836
	strand thickness [mm]	132.1
	strand width [mm]	984.0
	strand length [mm]	1200
	liquidus temperature [K]	1775
	solidus temperature [K]	1750
	latent heat [kJ/kg]	243
	density [kg/m ³]	7020
	thermal conductivity [W/m/K]	26
	specific heat [J/kg/K]	680
	material viscosity [kg/m/s]	5.55e-3
	density of particle [kg/m ³]	2700
	dendrite tip radius [μm]	3.3
steel grade 434 Cr steel		

Tab. 1: Geometrical and process parameters.

4. RESULTS

4.1 Melt Flow and Solidification

The steady flow pattern of the melt in the wide central plane is shown in Fig. 1. The liquid melt emerges from the inlet of the nozzle, divides through the trifurcated SEN into two side jets and one centre jet. The two side jets split at the narrow face of the mould and create the usual flow pattern, which includes an upper and a lower roll.

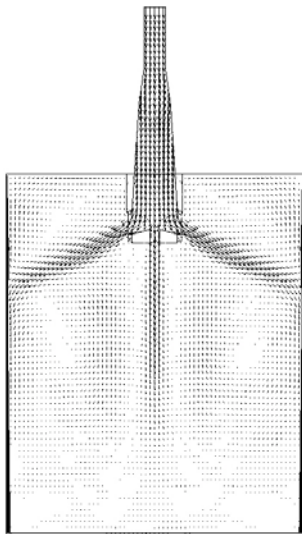


Fig. 1: Flow pattern in the wide centre plane. The black area shows the solidification zone.

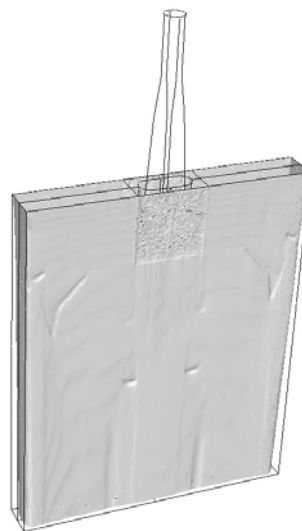


Fig. 2: Shape of the solidification front approximated with the iso-plane at a liquid fraction of $f_l = 0.9$.

Due to the drag of the dendrites, the flow slows down in the mushy zone and reaches the casting speed in the fully solid region. The flow pattern in this caster was validated with water models in [8]. The solidification shell is shown in Fig. 2 as an iso-surface of liquid fraction $f_l = 0.9$. It starts to build at the slag-melt interface and grows, depending on the cooling condition in the mould, while moving downwards. The unevenness is due to the influence of the flow, temperature and turbulence, which increases the thermal conductivity k_{eff} . The measurements of the shell thickness (Fig. 4, Fig. 5) on a breakout shell also show unevenness along the length. Due to the complexity of the geometry, a polyhedral mesh was chosen in and around the nozzle. This mesh effect causes unevenness of the shell in the quad-

atic region near the nozzle. However, the region affected by polyhedral elements is small compared to the remaining solidification area. The best results for modelling solidification were achieved with extremely fine and graded hexahedral elements. Grid refinement was done, especially in the vicinity of the solidification front. Grid independence was achieved using a grid of 1.2 million cells. The grid studies have also shown that mesh refinement is important, especially near the narrow faces of the mould, due to the high temperature and velocity gradients at the impingement area of the side jet.

The predictions of this model were compared with measurements on a breakout shell [9]. Values of the primary dendrite arm spacing along the slab length (from 58 μm to 145 μm) were also published in [9]. The calculated shell thickness at $f_l = 0.9$ are compared with the measurements at the wide and the narrow faces in Fig. 3 and Fig. 4. The calculated shell thickness is in good agreement with the measurements. The modelled narrow-face shell thickness has the same tendency and is only a few millimetres thinner. Also the measurements on both narrow faces (Fig. 4 dotted lines) differ by a similar magnitude. It seems that the calculated curve along the narrow face is shifted slightly to lower positions. A slight downward movement of the side jets in the real process could explain this. The reason for the steeper angle of the measured points from 0 to 200 mm below the meniscus could be due to the transient nature of the breakout [8].

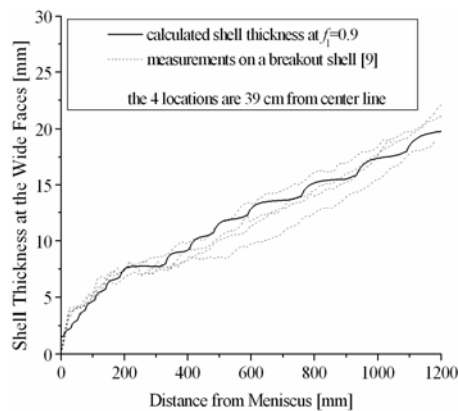


Fig. 3: Comparison of the calculated shell thickness on the wide faces with measurements.

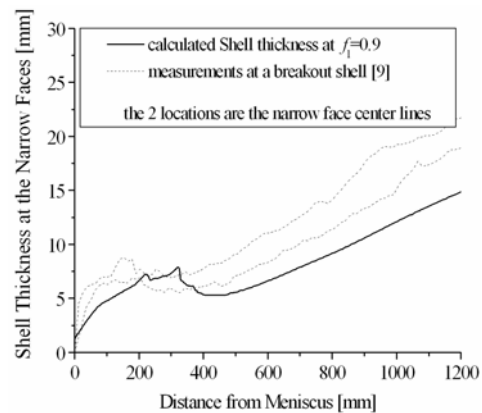


Fig. 4: Comparison of the calculated shell thickness on the narrow faces with measurements

4.2 Particle entrapment

After a steady state fluid flow and solidification solution has been achieved, 5000 particles of different particle size classes are injected from the top inlet of the nozzle. The distribution of entrapped or engulfed particles is shown in Fig. 5. Two different particle size classes (100 μm and 400 μm alumina inclusions) are shown. Capture on the inside and outside radius of this straight-mold caster is similar. Particles which are smaller than the primary dendrite arm spacing are directly entrapped. Depending on the local conditions at the dendrite front (liquidus isoline), particles bigger than the primary dendrite arm spacing are either engulfed or pushed away (reflected) from the mushy zone. All particles touching the slag-melt interface are assumed to be caught. The oversized black dots in Fig. 5 show the entrapment/engulfment positions of particles within the wide and narrow face mushy zone and within the casting slag. The grey background is the "solidification front", defined by $f_l = 0.9$. Our results predict a removal at the casting slag of 30 % of the bigger particles and of only 4.5 % of the smaller. The amount of entrapped or engulfed particles in the solidified strand is strongly influenced by the melt flow. High particle entrapment rates are located in areas where the three jets from the trifurcated nozzle approach the solid shell. For the smaller particles, $d_p = 100 \mu\text{m}$, the relative velocity between particles and melt caused by the buoyancy force is small, so that the particles in these jets are quickly brought to the solidification front before they are able to float up. The higher buoyancy force acting on bigger particles makes them float up easier. The model that decides whether particles are entrapped or pushed/engulfed depends on the particle diameter relative to the primary dendrite arm spacing. Lower than 450 mm below the meniscus (which is the centre of the lower roll of the side jets) the primary dendrite arm spacings become larger than the diameter of the

smaller particles, so that the smaller particles are easier to entrap. Different buoyancy and drag forces might increase or decrease the relative velocity between particles and shell. Entrapment is most probable if the particle has the same speed as the solid shell. Fig. 6 shows an example of particles being pushed at the liquidus isotherm for a “non-moving-solid” benchmark. Here, the vectors show the velocity of the melt.

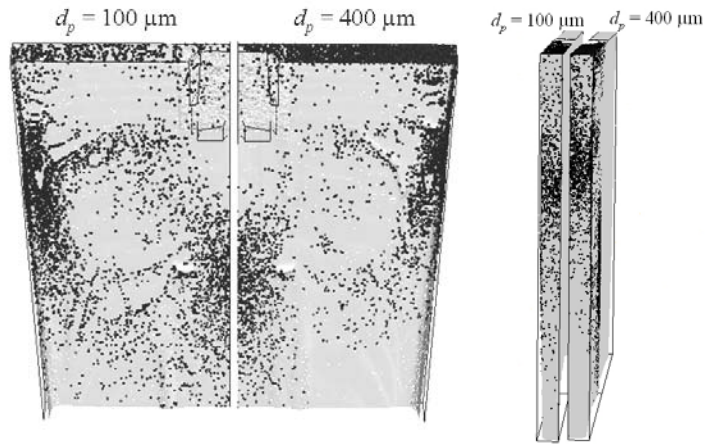


Fig. 5: Entrapped/ engulfed particle positions for $d_p = 100\mu\text{m}$ (left half) and $d_p = 400\mu\text{m}$ (right half) at the mushy zones ($f_l = 0.9$) and at the casting slag.

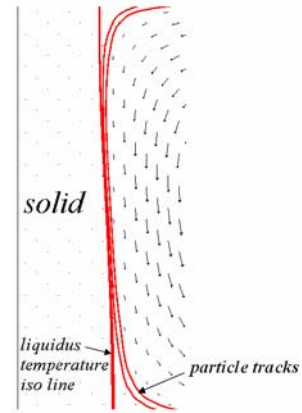


Fig. 6: Example of particle pushing

5. CONCLUSIONS

The presented numerical model combines turbulent melt flow, columnar solidification and particle transport, entrapment, engulfment and pushing. Reasonable agreement of the calculated shell thickness with experimental data using this single-phase solidification model was achieved. Simulations of flow and solidification can be done with this model within a moderate CPU time. However, an extremely fine grid, in and near the mushy zone is very important to achieve accurate predictions of the dendrite tip front envelope. By combining the solidification model with a dispersed particle model to estimate inclusion trajectories, and a particle capture/pushing model, the entrapment / engulfment positions of inclusions in the mushy zone of a steel continuous caster are predicted.

6. ACKNOWLEDGEMENTS

This work is financially supported by the Austrian Christian-Doppler (CD) Research Society, RHI AG, Technology Center Leoben and Siemens-VAI Linz for which the authors kindly acknowledge. The authors wish to express their appreciation to ANSYS Inc./FLUENT Inc. for their excellent technical assistance.

7. BIBLIOGRAPHIES

- [1] Voller, V. R. and Brent, A. D.: Applied Mathematical Modelling, 14 (1990), 320-326
- [2] Shangguan, D., Ahuja, S., Stefanescu, D.M.: Met. Trans. A, 23 (1992), 669-680
- [3] Kaptay, G.: Metallurgical and Materials Transactions A, 33 (2002), 1869-1873
- [4] Yuan, Q.: Transient Study of Turbulent Flow and Particle Transport During Continuous Casting of Steel Slabs. Department of Mechanical Engineering, University of Illinois, (2004)
- [5] Gu, J. P., Beckermann, C.: Metallurgical and Materials Transactions A, 30A (1999), 1357-1366
- [6] Pfeiler, C., Wu M., Ludwig, A., Chimani, C., Watzinger, J., Dösinger, H.: MCWASP XI, Opio, France, TMS (2006), 737-744
- [7] Crowe, C., Sommerfeld, M., Tsuji, Y.: Multiphase Flows with Droplets and Particles. CRC Press LLC (1998)
- [8] Thomas, B.G., O'Malley, R., Shi, T., Meng, Y., Creech, D., Stone, D.: MCWASP IX, Aachen, Germany, Shaker Verlag GmbH (2000), 769-776
- [9] Thomas, B.G., O'Malley, R., Stone, D.: Continuous Casting Consortium Progress Report (1998)